Volume 13
Number 10
21 May 2023
Pages 2867–3194

Catalysis Science & Technology

rsc.li/catalysis

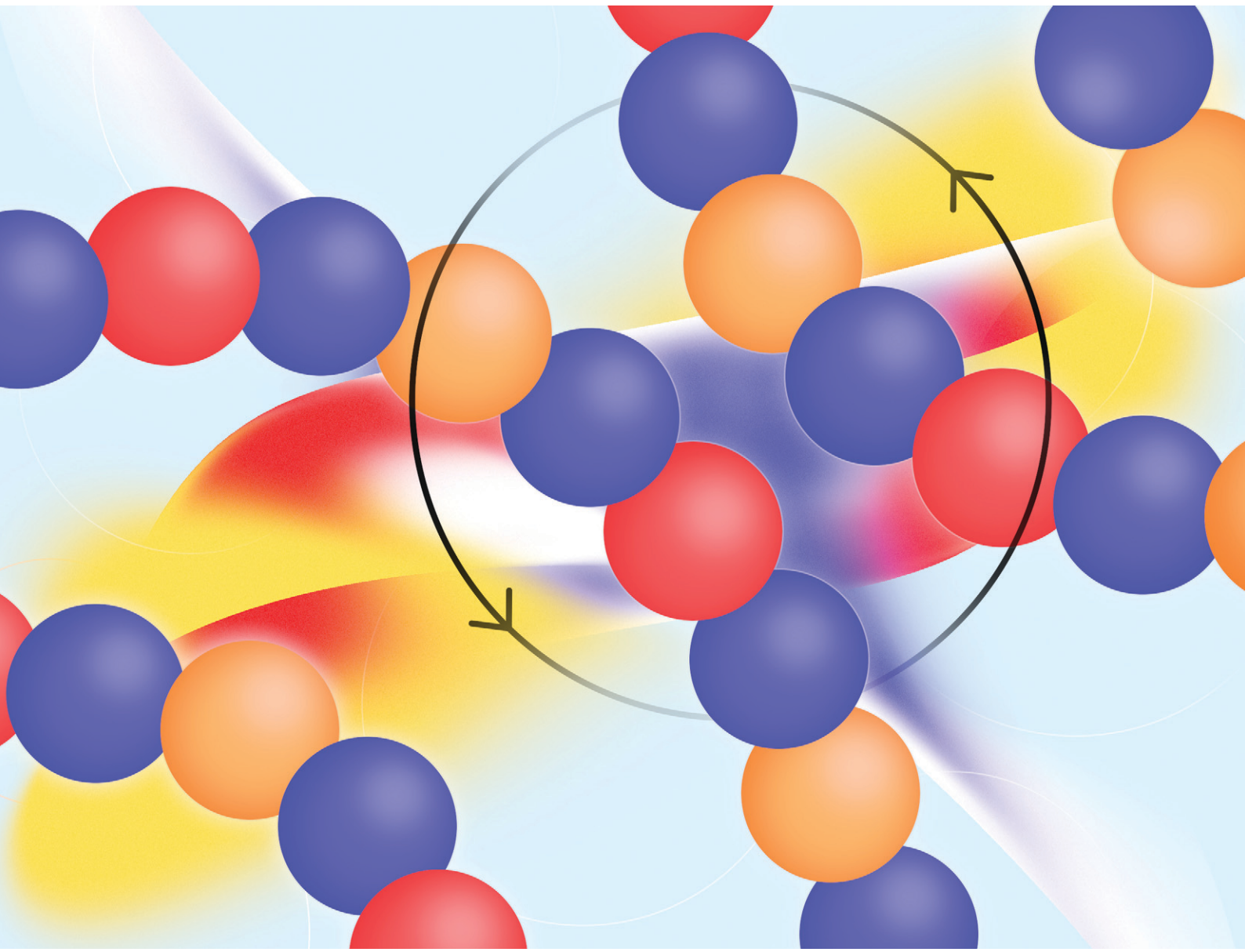

ISSN 2044-4761

ROYAL SOCIETY OF CHEMISTRY

PAPER
Peter Deglmann, Alex J. Plajer *et al.*
Lithium catalysed sequence selective ring opening terpolymerisation: a mechanistic study

Catalysis Science & Technology

ROYAL SOCIETY OF CHEMISTRY

PAPER

View Article Online
View Journal | View Issue

Open Access Article. Published on 10 April 2023. Downloaded on 10/26/2025 3:31:33 PM.
This article is licensed under a Creative Commons Attribution-NonCommercial 3.0 Unported Licence.

Check for updates

Cite this: *Catal. Sci. Technol.*, 2023, **13**, 2937

Lithium catalysed sequence selective ring opening terpolymerisation: a mechanistic study†

Peter Deglmann,*[a] Sara Machleit,[b] Cesare Gallizioli,[b] Susanne M. Rupf[b] and Alex J. Plajer *[b]

The catalytic construction of well-defined materials from mixtures of building blocks is an important challenge in sustainable catalysis. In this regard, we have recently reported a new type of selective ring-opening terpolymerisation (ROTERP), in which three monomers (A, B, C) are selectively enchained into a $(ABA'C)_n$ sequence, but the reasons behind this unusual selectivity remained unanswered. In this study, we present a detailed investigation into the full ROTERP mechanism based on the reactivity of model intermediates, computational studies investigating >100 possible intermediates and transition states and reaction kinetics. Experimental verification of the intermediate speciation, the primary insertion steps and the side-reactions lets us show that although most insertions and side-reactions are thermodynamically viable, kinetic selection processes at the propagating chain end determine the sequence selectivity. Computational studies elucidate the special role and speciation of the lithium catalyst which during the catalytic cycle involves mono-metallic, bi-metallic and charge separated transition states comprising both coordinative activation of incoming monomers and functional groups of the polymer backbone adjacent to the propagating chain. Our study not only deciphers the mechanism of a rare selective terpolymerisation but also helps answering open questions relevant to ring-opening copolymerisation (ROCOP) and alkali-metal catalysis in general, thus guiding the design of future polymerisation catalysis for degradable materials.

Received 2nd March 2023,
Accepted 6th April 2023

DOI: 10.1039/d3cy00301a

rsc.li/catalysis

Introduction

Controlled ways to make degradable and chemically complex materials from mixtures of building blocks are increasingly required in order to tailor their properties to ever more demanding technological requirements.[1–8] One popular methodology to achieve this is the alternating ring-opening copolymerisation (ROCOP) of a strained heterocycle with a heteroallene (yielding *e.g.* polycarbonates from CO_2 and epoxides) or a second heterocycle (yielding *e.g.* polyesters from cyclic anhydrides and epoxides).[9–16] Sustainable catalysts featuring main-group metals are enjoying increasing popularity, but the associated reaction pathways are only partially understood and it is often unclear which mono- or multimetallic, cooperative or uncooperative and neutral or zwitterionic routes occur.[17–25] Polymerising more complex ROCOP monomer mixtures with such catalysts can achieve the selective one-pot construction of higher order polymer architectures. For example, ternary mixtures comprising cyclic anhydrides, CO_2 and epoxides can be selectively polymerised into polyester-*b*-polycarbonate blockpolymers, *i.e.* CO_2/epoxide ROCOP only occurring once all anhydride is consumed and similar selectivities are observed for related monomer combinations.[4,26–34] Both insertion kinetics and intermediate thermodynamics have been proposed to be responsible for this selectivity which still remains under debate.[26,27,35–37] Moving down the periodic table, sulfur containing ROCOP monomer combinations likewise exist which mostly remain to be explored in terpolymerisation reactions.[33,38–45] Phthalic thioanhydride (PTA)/epoxide ROCOP for example yields poly[ester-*alt*-thioesters] while CS_2/epoxide ROCOP can yield poly(monothio-*alt*-trithiocarbonate) as reported by Werner and co-workers although the formal product of alternating ROCOP would be a poly(dithiocarbonate).[41,46–48] Combining these ROCOPs, we recently reported a lithium catalysed PTA/CS_2/epoxide ring-opening terpolymerisation (ROTERP, with propylene oxide (PO) or butylene oxide (BO)) and observed the formation of poly(ester-*alt*-ester-*alt*-trithiocarbonates) with a few erroneous thioester links (Fig. 1).[49–51] The ROTERP polymers were produced in an unusual (head-to-head)-*alt*-

[a] *BASF SE, Carl-Bosch-Strasse 38, 67056 Ludwigshafen am Rhein, Germany. E-mail: peter.deglmann@basf.com*
[b] *Institut für Chemie und Biochemie, Freie Universität Berlin, Fabeckstraße 34-36, 14195 Berlin, Germany. E-mail: plajer@zedat.fu-berlin.de*

† Electronic supplementary information (ESI) available. CCDC 2236905 and 2236906. For ESI and crystallographic data in CIF or other electronic format see DOI: https://doi.org/10.1039/d3cy00301a

Open Access Article. Published on 10 April 2023. Downloaded on 10/26/2025 3:31:33 PM.
This article is licensed under a Creative Commons Attribution-NonCommercial 3.0 Unported Licence.

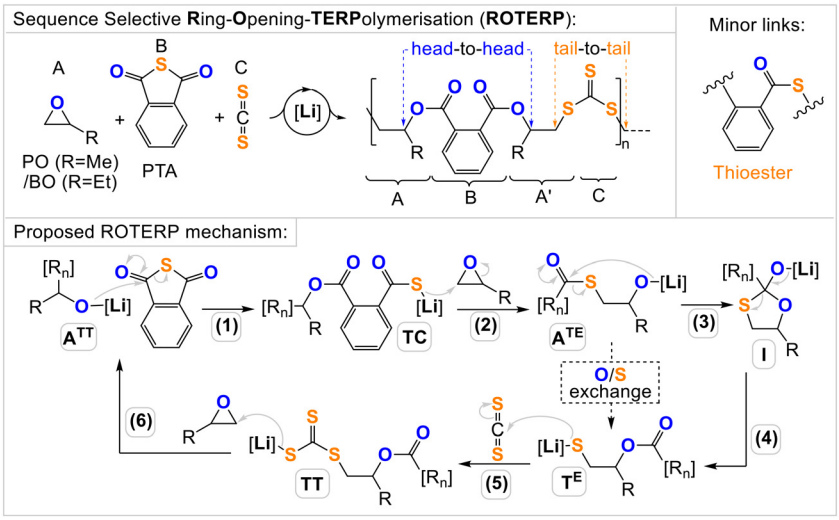

Fig. 1 PTA/CS_2/epoxide ROTERP and postulated propagation mechanism. R = Me, Et; R_n = polymer chain.

(tail-to-tail) regioselectivity meaning that the trithiocarbonate links sit adjacent to secondary CH_2 groups while the ester links sit adjacent to tertiary CH groups. This regioselectivity pointed towards a close mechanistic relation to Werner's CS_2/epoxide ROCOP (ESI† Fig. S1) which led us to propose the reaction mechanism displayed in Fig. 1. Starting from a lithium alkoxide intermediate $\mathbf{A^{TT}}$ insertion of PTA generates a lithium thiocarboxylate **TC** in propagation step (1). The intermediate **TC** then selectively attacks at the CH_2 position of another epoxide in reaction step (2) which is commonly termed a "tail" selective attack. This forms a secondary lithium alkoxide $\mathbf{A^{TE}}$ that sits adjacent to a thioester link. The lithium alkoxide $\mathbf{A^{TE}}$ intramolecularly attacks the adjacent thioester group in step (3) to form a tetrahedral intermediate **I**. This intermediate then collapses in reaction step (4) into an ester appended primary lithium thiolate $\mathbf{T^E}$ and the overall transformation of an alkoxide into a thiolate chain end has been termed O/S exchange. Propagation steps (2)–(4) also generates a link resulting from an isomerised epoxide (akin a virtual thiirane; A′ in Fig. 1) and an *ortho*-terephthalate link in which both esters sit adjacent to tertiary CH "head" groups of the ring-opened monosubstituted epoxides. $\mathbf{T^E}$ then inserts into CS_2 in reaction step (5) to generate a primary lithium trithiocarbonate **TT**. In the final propagation step, which closes the catalytic cycle, the primary **TT** ring opens another epoxide in reaction step (6) which regenerates the alkoxide $\mathbf{A^{TT}}$ from which the cycle started. Importantly as the ring opening event is again tail selective, it constructs a trithiocarbonate link in "tail-to-tail" stereoselectivity with two CH_2 groups next to it. However, the mechanism mostly remained a mere hypothesis in our previous report and many questions remained unanswered. Gratifyingly though, all proposed intermediates are synthetically accessible lithium salts which allows to study their reactivity. This represents a rare opportunity to synthetically study the reactivity of intermediates in such co/terpolymerisation processes as corresponding model intermediates in related catalyses are not easily synthetically accessible.[9] Combined with kinetics and detailed computational studies we here present an investigation into the full ROTERP mechanism. We reveal the origins of (i) the observed monomer selection processes at the chain end, (ii) the suppression and assistance of side processes leading to O/S exchange and erroneous links as well as (iii) the role of the Li catalyst and (iv) the energetic profile of the main propagation cycle.

Results and discussion

Monomer selection by $\mathbf{A^{TT}}$: step (1)

Our investigation starts from the lithium alkoxide **A** that serves as a model for a secondary lithium alkoxide at the propagating chain end (ESI† section S3). In step (1) of Fig. 1, $\mathbf{A^{TT}}$ selectively reacts with PTA over CS_2 or epoxides which are also present in the mixture and accordingly we attempted reaction of **A** with those in d_8-THF at room temperature. As shown in Fig. 2, **A** instantaneously reacts with PTA to yield the lithium thiocarboxylate **TC** (δ [R(C═O)SLi] = 216.0 ppm, δ [R(C═O)OR] = 169.2 ppm, $\tilde{\nu}$ (C═O) = 1701.5 cm^{-1}) and with CS_2 generating lithium dithiocarbonate **DT** (δ [RO(C═S)SLi] = 244.6 ppm, $\tilde{\nu}$ (C═S) = 1037.1 cm^{-1}) as confirmed by multinuclear NMR, IR and a yellow discolouration due to formation of the (C═S) chromophore. In contrast no reaction is observed between **A** and BO (which we employed as the model epoxide throughout the study due to its higher boiling point compared to PO) showing that epoxide insertion by the lithium alkoxide is associated with significantly higher barriers explaining the absence of ether linkages during ROTERP. However, this leaves the question unanswered why PTA is selected over CS_2 by **A** in ROTERP and this could either be due to insertion kinetics or intermediate thermodynamics. In terms of the latter, we found that CS_2 insertion into **A** to form **DT** is at least partially reversible. Heating of **DT** under dynamic vacuum at 80 °C for 1 min results in formation of **A** as visually indicated by a vanishing of the yellow colour and confirmed by ^{1}H and ^{7}Li

Open Access Article. Published on 10 April 2023. Downloaded on 10/26/2025 3:31:33 PM.
This article is licensed under a Creative Commons Attribution-NonCommercial 3.0 Unported Licence.

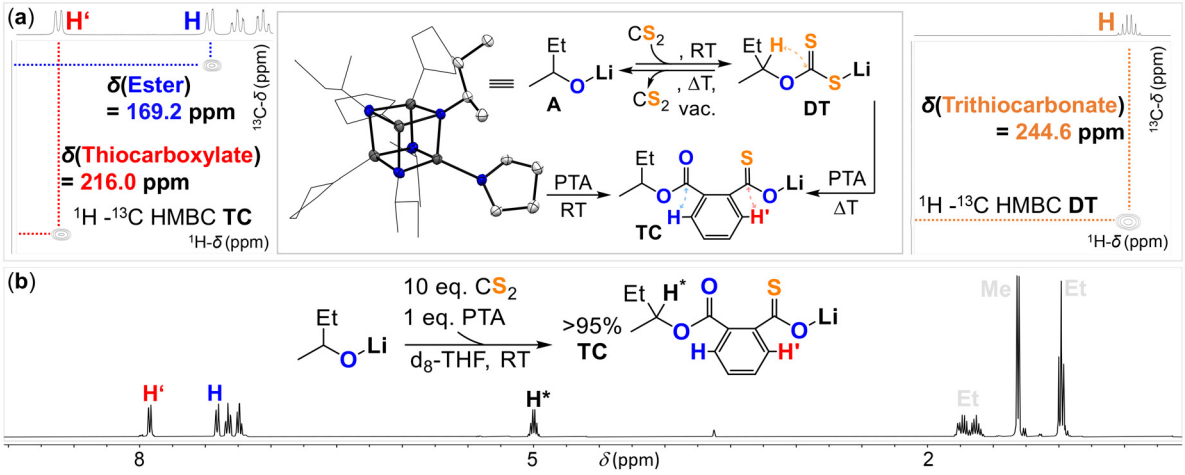

Fig. 2 (a) Reactivity and solid-state structure of model alkoxide **A**; ^{1}H–^{13}C HMBC (d_8-THF, 25 °C, 500 MHz) NMR spectra of **TC** and **DT**; (b) ^{1}H NMR spectrum (d_8-THF, 25 °C, 400 MHz) of products obtained from the reaction of **A** with a 10 : 1 mixture of CS_2 and PTA.

NMR. However, some insoluble decomposition products also form. Analogous attempts to revert PTA insertion into **A** starting from **TC** at high temperatures failed. If CS_2 into **A** is reversible but PTA insertion isn't, we hypothesized that transformation of **DT** into **TC** should be feasible. Addition of PTA to **DT** in d_8-THF initially results in no reaction at room temperature but heating to 80 °C overnight results in complete transformation to **TC**. This clearly indicates that PTA insertion from $\mathbf{A^{TT}}$ is the thermodynamically favoured propagation event. However, as ROTERP also occurs at room temperature with identical sequence selectivity and **DT** cannot be converted to **TC** at room temperature intermediate thermodynamics cannot be the only reason behind the insertion selectivity of $\mathbf{A^{TT}}$. To determine the kinetically favoured propagation step, we conducted a competition experiment in which we reacted **A** with a 10 : 1 mixture of CS_2 and PTA at room temperature in d_8-THF (note that a 10 CS_2 : 1 PTA ratio is also employed in the required monomer mixtures of ROTERP). Interestingly we see 96% selectivity for PTA insertion yielding **TC** and only 4% CS_2 insertion yielding **DT** although an excess of CS_2 was provided. We hence propose that lithium alkoxide $\mathbf{A^{TT}}$ selects PTA on kinetic grounds. Nevertheless, the same insertion is likewise favoured thermodynamically, and CS_2-PTA exchange could play a role at increased reaction temperatures.

O/S exchange: step (2)–(4)

Next up in the mechanism are steps (2)–(4) leading from **TC** to $\mathbf{T^E}$ *via* O/S exchange and these could be verified as thermodynamically favoured events in our previous report. Reacting **TC** with BO under a range of conditions always exclusively led to ester containing products and no thioesters from incomplete O/S exchange could be detected.[49] In order to then study reaction step (5) from species similar to $\mathbf{T^E}$, we prepared the primary lithium thiolate **T** adjacent to a tertiary carbon centre (ESI† section S4).

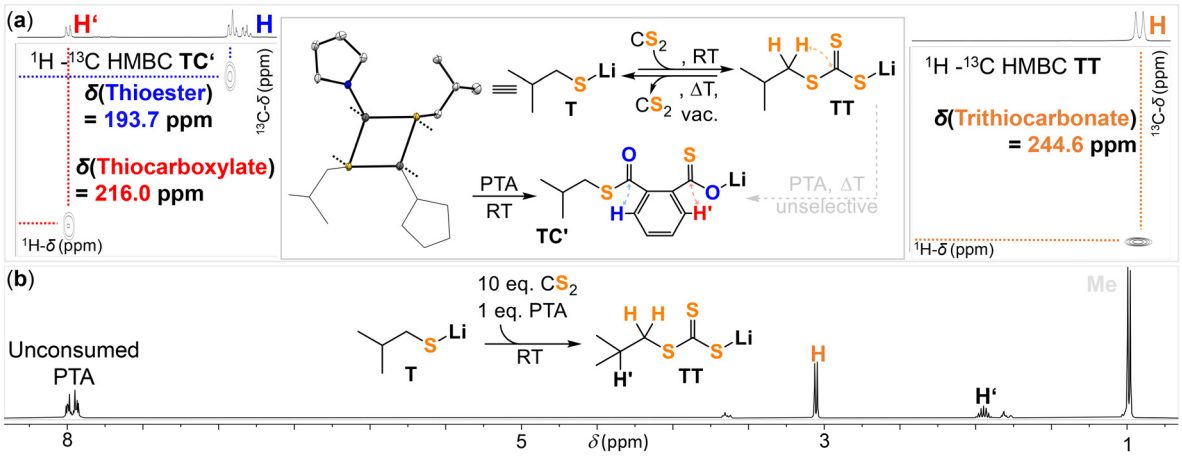

Fig. 3 (a) Reactivity and solid-state structure of model thiolate **T**; ^{1}H–^{13}C HMBC (d_8-THF, 25 °C) NMR spectra of **TT** and **TC'**; (b) ^{1}H NMR spectrum (d_8-THF, 25 °C, 400 MHz) of the reaction products of **T** with a 10 : 1 mixture of CS_2 and PTA.

Open Access Article. Published on 10 April 2023. Downloaded on 10/26/2025 3:31:33 PM.
This article is licensed under a Creative Commons Attribution-NonCommercial 3.0 Unported Licence.

Monomer selection by T^E: step (5)

As shown in Fig. 3, **T** instantaneously reacts with PTA to yield the lithium thiocarboxylate **TC′** (δ [R(C═O)SLi] = 216.0 ppm, $\tilde{\nu}$ = 1689.1 cm^{-1} and δ [R(C═O)SR] = 193.7 ppm, $\tilde{\nu}$ = 1556.3 cm^{-1}) and with CS_2 generating the lithium trithiocarbonate **TT** (δ [RS(C═S)SLi] = 244.6 ppm, $\tilde{\nu}$ = 996.5 cm^{-1}) as confirmed by multinuclear NMR, IR and a yellow discolouration due to the C═S chromophore. Since both CS_2 and PTA insertion are again possible from **T** this raises the question whether monomer selection in this step during ROTERP occurs on a thermodynamic or kinetic basis. Again, we found CS_2 insertion to be reversible. Heating **TT** at 80 °C under vacuum cleanly regenerates **T** as observed by ^1H and ^7Li NMR which is also visible by the disappearance of the yellow (C═S) chromophore. Reversible CS_2 insertion could again provide a pathway for CS_2 to PTA exchange. However, in contrast to **DT**, this reaction does not occur cleanly for **TT** and results in complex product mixtures. Although some PTA ring opening is observed indicating this insertion to be thermodynamically favoured over CS_2 insertion, monomer exchange pathways are unlikely to play a role during ROTERP and we thus investigated the potential for kinetic selection. Reacting **T** with a 10 : 1 mixture of CS_2 to PTA, which is the monomer ratio present during ROTERP, results in 99% selective CS_2 insertion yielding **TT**. We hence suggest the monomer selection in step (5) of Fig. 1 to occur on a kinetic basis; note that this is the opposite chemoselectivity that **A** shows. Surprisingly we observe ring opening of BO by **T** to form thioethers in d_8-THF at room temperature. However only trace amounts of thioether links are formed during ROTERP and this is likely because of faster CS_2 than BO insertion. Accordingly reacting **T** with a 2 : 1 mix of CS_2 and BO resulted in no thioether and only heterocarbonate formation. Another aspect concerning T^E is the origin of erroneous thioester links (Fig. 1) which either form from T^E if it inserts PTA or if A^{TE} propagates without O/S exchange. However, we previously found O/S exchange from **TC** to always occur quantitatively after BO insertion, making this thioester formation pathway unlikely.[49] On the other hand, we observed that lower CS_2 loadings in the starting monomer feed result in more thioester errors making PTA over CS_2 insertion from T^E the more likely mechanistic origin of errors. Seeking to confirm this hypothesis we conducted are series of competition experiments like those depicted in Fig. 3b in which **T** was combined with mixtures of 1 eq. PTA and 5 eq., 2 eq. or 1 eq. CS_2 in d_8-THF. In contrast to the competition experiment featuring a 1 : 10 PTA : CS_2 ratio, we observe PTA ring opening to an increasing extent as the amount of CS_2 is lowered. Hence kinetic CS_2 over PTA selection by the thiolate **T** is not achieved at lower relative CS_2 concentrations making erroneous PTA insertion by the thiolate intermediate **T** the likely origin of thioester errors.

Propagation from TT: step (6)

Closing the loop, we confirmed reaction step (6) by reacting **TT** with BO leading to organic heterocarbonate formation (Fig. 4b, ESI† section S5). This however leads to O/S scrambled heterocarbonate links rather than to clean formation of a trithiocarbonate appended lithium alkoxide like A^{TT} demonstrating that O/S exchange from A^{TT} (Fig. 4a) is thermodynamically feasible at room temperature. Accordingly, suppression of O/S exchange from A^{TT} must be a kinetic effect which we confirmed by reaction of **TT** with 1 eq. BO in presence of 1 eq. PTA cleanly generating the

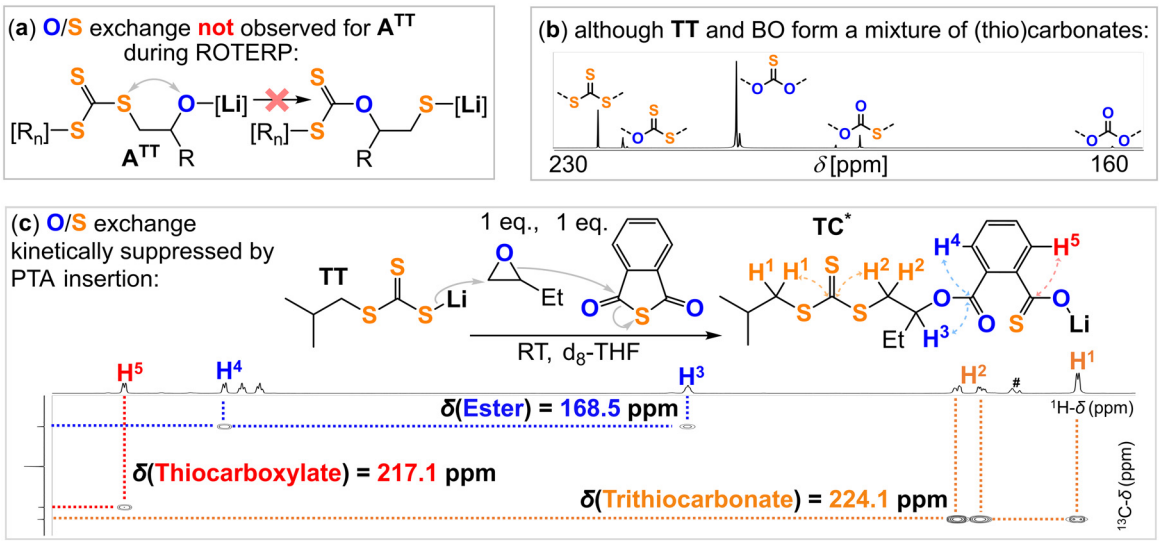

Fig. 4 (a) Formal O/S exchange from A^{TT} not observed during ROTERP; (b) reaction of **TT** with 1 eq. BO in d_8-THF leads to O/S scrambled organic heterocarbonates (^{13}C (126 MHz, d_8-THF, 25 °C) NMR spectra of the reaction mixture displayed) showing that O/S exchange is thermodynamically feasible; (c) consecutive enchainment of PTA, following BO insertion by **T** suppresses O/S exchange; ^1H–^{13}C HMBC spectrum (d_8-THF, 25 °C) and corresponding ^1H and ^{13}C NMR spectra of **TC***. #Denotes residual THF and d_8-THF signals.

Open Access Article. Published on 10 April 2023. Downloaded on 10/26/2025 3:31:33 PM.
This article is licensed under a Creative Commons Attribution-NonCommercial 3.0 Unported Licence.

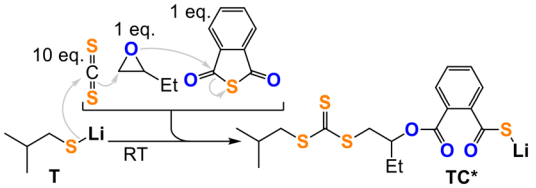

Fig. 5 Four component cascade reaction generating TC* from T, CS_2, BO and PTA.

lithium thiocarboxylate **TC*** (Fig. 4c). NMR and IR analysis of the obtained product clearly shows the generation of an organic trithiocarbonate (δ [RSC(═S)SR] = 224.1 ppm, $\tilde{\nu}$ = 1054.0 cm^{-1}) and an ester link (δ [RC(═O)OR] = 168.5 ppm, $\tilde{\nu}$ = 1700.0 cm^{-1}) as well as a lithium thiocarboxylate chain end (δ [RC(═O)SLi] = 217.1 ppm) and tail-selectively ring-opened BO. Going one step further, all selection processes occurring in steps (1) to (5) (Fig. 1) can be coupled to each other as shown in Fig. 5. Here, we reacted **T** with a mixture of 10 eq. CS_2, 1 eq. PTA and 1 eq. BO to likewise form the thiocarboxylate **TC*** while preserving the unscrambled trithiocarbonate link.

The rate determining step of ROTERP

Finally, we were wondering what the rate determining step of ROTERP is and at which type of chain end the lithium catalyst hence rests (ESI† section S6). Following the PTA consumption during ROTERP by ^{1}H NMR of aliquots removed at regular time intervals (Fig. 6(a)) reveals a linear dependence of PTA consumption *versus* time. This supports a 0th order dependence of the reaction rate regarding PTA further supporting that lithium alkoxides like $\mathbf{A^{TT}}$ are unlikely to be the resting states of ROTERP. We previously showed experimentally that ester appended lithium thiolates like $\mathbf{T^E}$ are unstable due to rapid thiirane elimination and that thioester appended lithium alkoxides like $\mathbf{A^{TE}}$ are unstable intermediates due to rapid O/S exchange.[49] Hence there remains the question whether BO insertion from **TC** in step (2) or from **TT** in step (6) is faster. We therefore performed a competition experiment in which we reacted a 1 : 1 mixture of **TC** and **TT** with 1 eq. BO in d_8-THF/CS_2 at room temperature. Under these conditions negligible reaction of **TC** occurs whereas **TT** reacts to form organic heterocarbonates (Fig. 6(b)) by BO insertion and initiation of CS_2/BO coupling. We then compared the reaction kinetics of PTA/CS_2/BO ROTERP with that of the parent PTA/BO and CS_2/BO ROCOP reactions which complemented our findings (Fig. 6(c)). Here we tracked the reaction progress of Li catalysed PTA/CS_2/BO ROTERP (at 1 eq. LiOBn: 100 eq. PTA: 800 eq. BO: 1600 eq. CS_2), CS_2/BO ROCOP (at 1 eq. LiOBn: 800 eq. BO: 1600 eq. CS_2) and PTA/BO ROCOP (at 1 eq. LiOBn: 100 eq. PTA: 800 eq. BO) employing an equal volume of toluene in place of CS_2 to reach comparable reactant concentrations. The reaction kinetics at room temperature assessed by ^{1}H NMR aliquot analysis as shown in Fig. 6(c) reveal that ROTERP

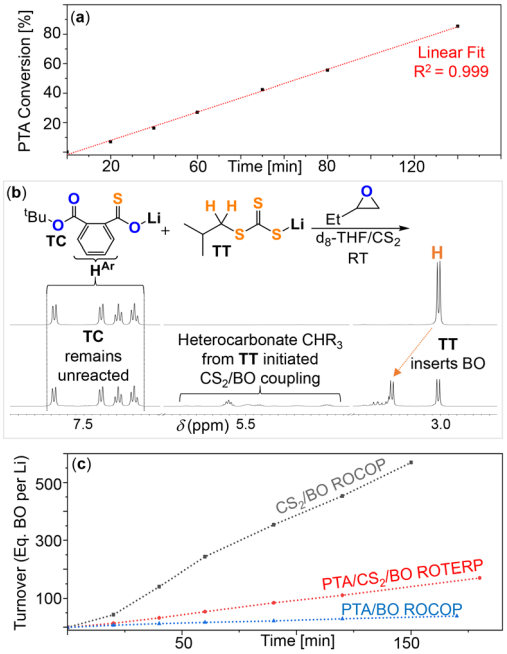

Fig. 6 (a) Linear fit of the PTA conversion *vs.* time at 1 eq. LiOBn: 100 eq. PTA: 800 eq. BO: 1600 eq. CS_2 at RT. (b) Competition experiment reacting a 1 : 1 mixture of **TC** and **TT** with 1 eq. BO at room temperature in d_8-THF (overlaid 400 MHz ^{1}H NMR shown); note that the previously reported ^{t}Bu derivative of **TC** was employed to avoid signal overlap.[49] (c) Comparison of the BO turnover *versus* time for ROTERP and the two parent ROCOP reactions as outlined in the main text; TOF as discussed in the main text obtained by linear fitting over the entire displayed range.

(TOF *ca.* 59 h^{-1}) is slower than CS_2/BO ROCOP (*ca.* 234 h^{-1}) but faster than PTA/BO ROCOP (*ca.* 13 h^{-1}) under comparable reaction conditions with regards to BO turnover. This suggests that reaction steps during ROTERP like PTA/BO ROCOP (*i.e.* PTA insertion and BO insertion from **TC**) are slower than the ones like CS_2/BO ROCOP (*i.e.* CS_2 insertion and BO insertion from **TT**). As ROTERP is 0th order in PTA this leaves BO insertion from **TC** as the slowest reaction step as indicated by our prior model intermediate studies. We therefore propose that the intermediate **TC** is the likely resting state of ROTERP. Furthermore, the experiment outlined in Fig. 5 can be viewed as a ROTERP at high Li-initiator loading (*i.e.* 100 mol%) as all monomer are present which are enchained to the **TC*** oligomer. Hence this provides direct spectroscopic evidence for the thiocarboxylate chain-end in the resting state of the ROTERP which confirms the conclusions made in this paragraph.

Density functional theory

With a mechanistic idea of monomer incorporation selectivity, side reactions and intermediate speciation at hand we turned to DFT modelling to shed light on the catalytic cycle and the nature of transition states as well as the exact nature and role of the Li centres which is otherwise hard to elucidate (ESI† section S8). The fact that heavier alkali metals

Open Access Article. Published on 10 April 2023. Downloaded on 10/26/2025 3:31:33 PM.
This article is licensed under a Creative Commons Attribution-NonCommercial 3.0 Unported Licence.

Na and K show worse or no appreciable activity/selectivity in ROTERP implies that Li acts as a true catalyst rather than a mere spectator counter cation. Quantum chemical computations were performed with the program package TURBOMOLE at a meta-hybrid DFT level of theory employing conformational searches and structure optimizations at the TPSSH/def-TZVP level (using the solvation model COSMO and assuming a dielectric constant of infinity) followed by M06-2X/def2-TZVPD single-point calculations.[52–58] For the final Gibbs free energies G given here, the solvation model COSMO-RS was used assuming as solvent a 2 : 1 mixture (by molarity) of CS_2 and PO; a temperature of 80 °C was assumed for this solvation treatment as well as for computing the statistic thermodynamics contributions to allow for an optimal comparison with our initial work.[49,59] For all transition states, it was checked which combination of reactants and products they actually link together by slight distortions (corresponding to 30 K) along both directions of the imaginary vibrational mode and subsequent structural relaxation. Before entering into the discussion of our computational results, we would like to point out that identification of reaction intermediates and transition states is non-trivial due to the manifold of possible ligands for coordination to the Li centres, which can be chain-ends, functional groups of the polymer chain adjacent to the chain-ends and the monomers. With respect to monomer coordination, it could be shown that PO (as a model alkylene oxide) binds more strongly than CS_2 as well as PTA, so that in the results shown in the following always PO was used to saturate available coordination sites at Li. It became also obvious that phthalic diester groups of the product are in spite of their chelating nature not superior as ligands compared to two PO, so that coordination to remote functional groups of the propagating chain or groups of other polymer chains is not expected (see ESI†). Another complication represents the tendency of lithium salts to aggregate into dimers and even more aggregated structures in solution. The most favoured intermediates and transition states from a Gibbs free energy perspective were identified assessing over 100 potential species for all of which searches for the lowest energy conformer at the level of structure optimization were performed; the reader is referred to the ESI† for a summary of the structures and their associated Gibbs free energies. Despite of these efforts, our investigations cannot deliver an exhaustive list of all possible lithium complexes involved in the ROTERP cycle, but rather

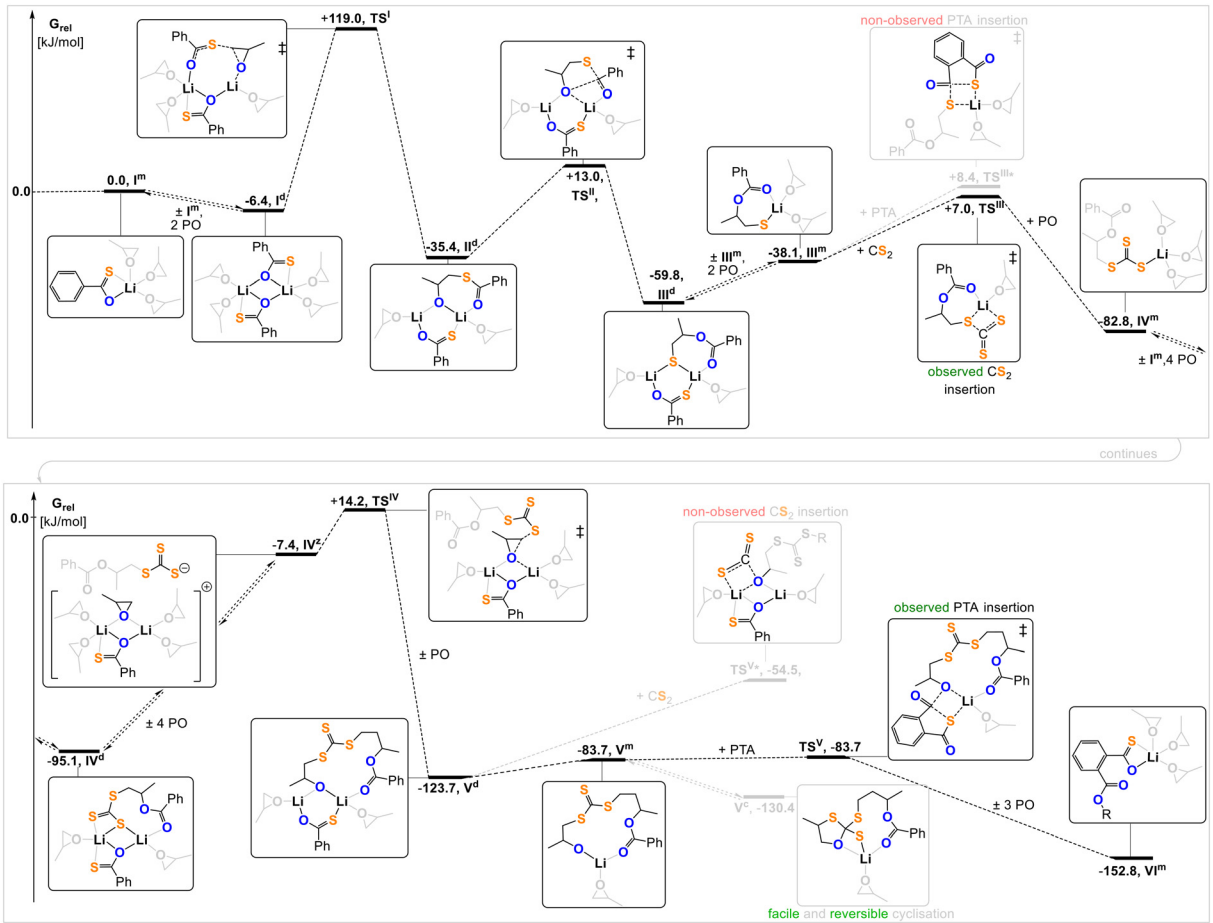

Fig. 7 Energy profile for the ROTERP propagation cycle computed on the M06-2X/def2-TZVPD||TPSSH/def-TZVP/COSMO($\varepsilon = \infty$) level of theory.

Open Access Article. Published on 10 April 2023. Downloaded on 10/26/2025 3:31:33 PM.
This article is licensed under a Creative Commons Attribution-NonCommercial 3.0 Unported Licence.

deliver one possible reactive pathway which nevertheless allows to draw some general conclusions about the transition state geometries, intermediate speciation, and the role of the lithium catalyst. A summary of the computed catalytic cycle is given in Fig. 7. The starting point represents the suspected lithium thiocarboxylate resting state in its monomeric form $\mathbf{I^m}$ for which coordination of three additional epoxides results in the most stable monomeric structure. We used thiobenzoate as a model polymer chain end and propylene oxide as model alkylene oxide throughout this study for reasons of computational simplicity. Aggregation to $\mathbf{I^d}$ results in a slightly more stable dimeric structure with a Li_2O_2 core bridged by the thiocarboxylate oxygens. It should be mentioned here, that for all aggregation equilibria, lithium thiocarboxylates were inferred as reagent, as these represent the suspected chain ends in the resting state of the catalytic cycle and must therefore be primarily available in the reaction mixture. From $\mathbf{I^d}$, ring opening occurs through a bimetallic transition state $\mathbf{TS^I}$ ($\Delta G^{\ddagger}$ = 125.4 kJ mol^{-1}) in which the reacting thiocarboxylate is coordinated by one Li while the inserted PO ring is coordinatively activated by the second Li centre. It should be noted that tail-selective PO ring-opening at the CH_2 position is energetically most favourable as it represents the S_N2 reaction at the less substituted carbon atom. Monometallic PO ring-opening transition states starting from $\mathbf{I^m}$ result in significantly higher $\Delta G^{\ddagger}$ as a consequence of the angular constraints around the attacked C-atom at which in S_N2 reactions nucleophile and leaving group optimally assume an angle of 180°. Further bimetallic transition states in which two monomeric units are not linked by an anionic bridging ligand are likewise less favoured as a consequence of the fact that either reactant or product have to be of zwitterionic nature. $\mathbf{TS^I}$ leads to a dimeric intermediate $\mathbf{II^d}$ with the thiocarboxylate bridging through the O and S centres (generally, μ^2- or κ^2-bridging by either O only or O and S, respectively, was found to be energetically quite close for thiocarboxylate links between two Li) as well as a bridging alkoxide. Notably the carbonyl oxygen of the adjacent thioester link coordinates in this most stable form of $\mathbf{II^d}$ to one of the Li centres and this already hints the subsequent activation of the thioester group for nucleophilic attack in the O/S exchange step. Intramolecular attack ($\Delta G^{\ddagger}$ = 48.4 kJ mol^{-1}) of the thioester by the alkoxide *via* $\mathbf{TS^{II}}$ transforms the alkoxide into a thiolate and this exchange step is orders of magnitude-faster than the PO ring-opening before (and expected to be also faster than any reaction with CS_2 or PTA, when comparing the analogous differences in Gibbs free energies between $\mathbf{V^d}$ and transition states $\mathbf{TS^V}$ or $\mathbf{TS^V}$*). $\mathbf{TS^{II}}$ actually represents the initial alkoxide attack to form as primary product a tetrahedral intermediate in which the two O-atoms as in the transition state are linked to Li; however, any attempt of optimizing analogous species with the negatively charged O and S coordinated to Li – as a prerequisite for thiolate formation – led to spontaneous C–S bond cleavage, so that it can be concluded that this carbonyl addition–elimination reaction is limited by the addition step and that elimination is fast and does not require more than dissociation of a neutral donor atom from Li and coordination of another. Notably the thiolate $\mathbf{III^d}$ is 24.4 kJ mol^{-1} more stable than its alkoxide counterpart $\mathbf{II^d}$ demonstrating that O/S exchange at the chain-end is a thermodynamically favourable process. Monometallic O/S exchange transition states starting from monomeric lithium alkoxides lead to significantly higher barriers, which fits to the general observation that the strongly coordinating alkoxide anion has a high preference for dinuclear species which is much less pronounced for less coordinating anions like thiolate or anions with negative charge delocalization like thiocarboxylates or trithiocarbonates. Moreover, transition states similar to $\mathbf{TS^{II}}$ for which the thiocarboxylate spectator ligand acts as a μ^2-bridge *via* O only (instead of κ^2-bridging *via* O and S) also lie energetically higher, which results from the fact that the corresponding structures contain too many small rings annulated with each other, showing that a modulation of the Li···Li separation through different bridging modes of the thiocarboxylates plays a role in the ROTERP mechanism. From $\mathbf{III^d}$ CS_2 insertion has to occur in order to continue propagation, however in this case bimetallic transition states are less favoured than monometallic ones. We infer that this is partially due to steric encumbrance of the thiolates by the two flanking Li centres which also withdraw electron density from the nucleophilic S. In order to achieve monometallic CS_2 insertion, fragmentation of the dimers $\mathbf{III^d}$ into their monomeric form $\mathbf{III^m}$ under coordination of an additional equivalent of PO per Li occurs, overall requiring 21.7 kJ mol^{-1}. The four-membered transition state $\mathbf{TS^{III}}$ ($\Delta G^{\ddagger}$ = 45.1 kJ mol^{-1} with respect to $\mathbf{III^m}$) that leads to CS_2 insertion also lies from a free energy perspective lower than the prior PO ring-opening. Importantly CS_2 insertion is only associated with a slightly lower barrier than PTA insertion ($\mathbf{TS^{III}}$*, $\Delta G^{\ddagger}$ = 46.5 kJ mol^{-1}) confirming that although CS_2 insertion is kinetically favoured, monomer selection by the lithium thiolate chain end is also concentration driven and requires a large excess of CS_2 as found in our experimental studies in order to achieve highly regular product structures. These findings also explain that erroneous PTA insertion from lithium thiolates *via* $\mathbf{TS^{III}}$* cause the aforementioned thioester errors. Progressing in the catalytic cycle, $\mathbf{TS^{III}}$ leads to the lithium trithiocarbonate $\mathbf{IV^m}$ which then undergoes the thermodynamically slightly favourable dimerization to $\mathbf{IV^d}$ with a thiocarboxylate $\mathbf{I^m}$. Surprisingly from here the energetically most favourable PO ring-opening pathway involves initial dissociation of the trithiocarbonate ligand under additional PO coordination to form the zwitterionic intermediate $\mathbf{IV^z}$ (the given free energy refers to then solvent separated ion pair) which lies energetically uphill by 87.7 kJ mol^{-1} compared to $\mathbf{IV^d}$. This ligand exchange at Li effectively swaps a μ^2-S for a μ^2-O donor and could be facilitated by the high oxophilicity of Li. PO ring-opening in $\mathbf{TS^{IV}}$ from here occurs with a very small additional activation barrier ($\Delta G^{\ddagger}$ = 24.4 kJ mol^{-1}) so that the overall barrier for PO ring-opening

Open Access Article. Published on 10 April 2023. Downloaded on 10/26/2025 3:31:33 PM.
This article is licensed under a Creative Commons Attribution-NonCommercial 3.0 Unported Licence.

starting from $\mathbf{IV^d}$ that needs to be overcome amounts to 112.1 kJ mol^{-1}. PO ring-opening by the lithium trithiocarbonate from $\mathbf{IV^d}$ to $\mathbf{V^d}$ is therefore predicted to occur more easily by 13.3 kJ mol^{-1} than PO ring-opening by lithium thiocarboxylates, confirming $\mathbf{TS^I}$ to be the rate-determining step of the reaction. The zwitterionic nature of the most favourable $\mathbf{TS^{IV}}$ can be understood as a consequence of the generally weaker binding between Li and trithiocarbonate anions compared to thiocarboxylates (as can be seen in the ESI by comparing the speciation of **I** and **IV**). From here, several possible propagation pathways with PTA are possible; in case of the monometallic ones some of the most favourable ones are actually barrierless, *i.e.* are spontaneous reactions once the corresponding monometallic precursor with a free coordination site has been generated by the energetically uphill (ΔG = 40.0 kJ mol^{-1}) dissociation of dimers $\mathbf{V^d}$ into monomers $\mathbf{V^m}$ (see ESI† for more details) and this is in line with the experimentally determined 0th reaction order in PTA concentration; in cases with more steric crowding around Li, PTA inserts in a four-membered transition state $\mathbf{TS^V}$, which however does not seem the most favoured option. In contrast, CS_2 insertion occurs most easily starting directly from $\mathbf{V^d}$ with an insertion barrier to $\mathbf{TS^{V}}$* of $\Delta G^{\ddagger}$ = 69.2 kJ mol^{-1} confirming that PTA insertion is in fact kinetically favoured from this alkoxide intermediate that does – because of the more different barriers involved – less depend on monomer concentration than the competition of $\mathbf{TS^{III}}$ and $\mathbf{TS^{III*}}$. One final question concerns the circumstance why no O/S exchange occurs from $\mathbf{V^m}$ (corresponding to $\mathbf{A^{TT}}$ in Fig. 1). In this regard a cyclised variant $\mathbf{V^c}$ observed without explicitly searching for it upon a conformational scan of $\mathbf{V^m}$ suggests that cyclization initiating the O/S exchange process is a possible (and obviously reversible) process that occurs with a negligible barrier. In two cases it was found, that releasing a dialkyl dithiocarbonate and a thiolate chain end from this is actually slightly exergonic with respect to dialkyl trithiocarbonate and alkoxide chain end. However, from the activation barriers computed for $\mathbf{TS^{III}}$, one would expect the corresponding transition states of CS_2 addition around 20 kJ mol^{-1} higher (see ESI† for **V**) than the most favourable $\mathbf{TS^V}$. As PTA insertion is irreversible (*vide supra*), any $\mathbf{V^m}$ is thus in the presence of PTA rapidly scavenged which suppresses any O/S scrambling as predicted by our model intermediate studies.

Conclusions

In conclusion, we have presented a thorough experimental verification of the intermediate speciation, the propagation events, and the side processes of the ROTERP reaction mechanism. We found that although most insertions and side processes are thermodynamically feasible a series of kinetic selection processes at the propagating chain-end determine the ROTERP sequence selectivity. Nevertheless, as CS_2 insertion is reversible, erroneous insertions can be corrected at elevated temperatures. Although O/S scrambling pathways are thermodynamically favoured for alkoxide chain ends adjacent to sulfurated links, these are kinetically suppressed for alkoxides adjacent to trithiocarbonate links by propagation. Furthermore, we identified epoxide ring opening following PTA insertion as the rate-determining step. Our computational investigations helped to elucidate the special role of the Li catalyst. ROTERP is enabled by fluxional aggregation at the chain end allowing for mono and multimetallic insertion steps and is furthermore facilitated by a certain degree of plasticity of the intermetallic distance through different bridging ligands and adaptable bridging modes of those. The high oxophilicity of lithium leads to coordinative activation of carbonyl groups adjacent to the chain-end as well as formation of zwitterionic intermediates enabling the associated transition states. All these factors collaboratively enable the polymerisation process which has been oversimplified in the past. Our results demonstrate how exactly sustainable main-group metals enable the selective catalytic synthesis of degradable heteroatom-containing polymers and provide guidance for future catalyst selection and unprecedented polymer sequence and architecture design.

Conflicts of interest

There are no conflicts of interest.

Acknowledgements

The VCI is acknowledged for a Liebig Fellowship for A. J. P. and a Ph.D. scholarship for C. G. Prof. Dr Christian Müller and Prof. Dr Rainer Haag are thanked for continuous support and valuable discussions.

References

1 T. P. Haider, C. Völker, J. Kramm, K. Landfester and F. R. Wurm, *Angew. Chem., Int. Ed.*, 2019, **58**, 50–62.
2 J.-F. Lutz, M. Ouchi, D. R. Liu and M. Sawamoto, *Science*, 2013, **341**, 1238149.
3 N. Badi and J.-F. Lutz, *Chem. Soc. Rev.*, 2009, **38**, 3383–3390.
4 A. C. Deacy, G. L. Gregory, G. S. Sulley, T. T. D. Chen and C. K. Williams, *J. Am. Chem. Soc.*, 2021, **143**, 10021–10040.
5 C. Hu, X. Pang and X. Chen, *Macromolecules*, 2022, **55**, 1879–1893.
6 C. M. Bates and F. S. Bates, *Macromolecules*, 2017, **50**, 3–22.
7 F. S. Bates, M. A. Hillmyer, T. P. Lodge, C. M. Bates, K. T. Delaney and G. H. Fredrickson, *Science*, 2012, **336**, 434–440.
8 F. M. Haque, J. S. A. Ishibashi, C. A. L. Lidston, H. Shao, F. S. Bates, A. B. Chang, G. W. Coates, C. J. Cramer, P. J. Dauenhauer, W. R. Dichtel, C. J. Ellison, E. A. Gormong, L. S. Hamachi, T. R. Hoye, M. Jin, J. A. Kalow, H. J. Kim, G. Kumar, C. J. LaSalle, S. Liffland, B. M. Lipinski, Y. Pang, R. Parveen, X. Peng, Y. Popowski, E. A. Prebihalo, Y. Reddi, T. M. Reineke, D. T. Sheppard, J. L. Swartz, W. B. Tolman, B. Vlaisavljevich, J. Wissinger, S. Xu and M. A. Hillmyer, *Chem. Rev.*, 2022, **122**, 6322–6373.
9 A. J. Plajer and C. K. Williams, *Angew. Chem., Int. Ed.*, 2022, e202104495.

 This journal is © The Royal Society of Chemistry 2023

Open Access Article. Published on 10 April 2023. Downloaded on 10/26/2025 3:31:33 PM.
This article is licensed under a Creative Commons Attribution-NonCommercial 3.0 Unported Licence.

10 G.-W. Yang, C.-K. Xu, R. Xie, Y.-Y. Zhang, C. Lu, H. Qi, L. Yang, Y. Wang and G.-P. Wu, *Nat. Synth.*, 2022, 1–10.
11 Y. Popowski, Y. Lu, G. W. Coates and W. B. Tolman, *J. Am. Chem. Soc.*, 2022, **144**, 8362–8370.
12 J. Schaefer, H. Zhou, E. Lee, N. S. Lambic, G. Culcu, M. W. Holtcamp, F. C. Rix and T.-P. Lin, *ACS Catal.*, 2022, **12**, 11870–11885.
13 Y. Yu, B. Gao, Y. Liu and X.-B. Lu, *Angew. Chem., Int. Ed.*, 2022, e202204492.
14 A. J. Plajer and C. K. Williams, *ACS Catal.*, 2021, **11**, 14819–14828.
15 W. Gruszka and J. A. Garden, *Nat. Commun.*, 2021, **12**, 3252.
16 J. Xu and N. Hadjichristidis, *Angew. Chem., Int. Ed.*, 2021, **60**, 6949–6954.
17 X. Xia, R. Suzuki, K. Takojima, D.-H. Jiang, T. Isono and T. Satoh, *ACS Catal.*, 2021, **11**, 5999–6009.
18 X. Xia, R. Suzuki, T. Gao, T. Isono and T. Satoh, *Nat. Commun.*, 2022, **13**, 163.
19 X. Xia, T. Gao, F. Li, R. Suzuki, T. Isono and T. Satoh, *J. Am. Chem. Soc.*, 2022, **144**, 17905–17915.
20 Y. Reddi and C. J. Cramer, *ACS Catal.*, 2021, **11**, 15244–15251.
21 D. Zhang, S. K. Boopathi, N. Hadjichristidis, Y. Gnanou and X. Feng, *J. Am. Chem. Soc.*, 2016, **138**, 11117–11120.
22 M. E. Fieser, M. J. Sanford, L. A. Mitchell, C. R. Dunbar, M. Mandal, N. J. Van Zee, D. M. Urness, C. J. Cramer, G. W. Coates and W. B. Tolman, *J. Am. Chem. Soc.*, 2017, **139**, 15222–15231.
23 B. A. Abel, C. A. L. Lidston and G. W. Coates, *J. Am. Chem. Soc.*, 2019, **141**, 12760–12769.
24 L. Song, M. Liu, D. You, W. Wei and H. Xiong, *Macromolecules*, 2021, **54**, 10529–10536.
25 D. Zhang, H. Zhang, N. Hadjichristidis, Y. Gnanou and X. Feng, *Macromolecules*, 2016, **49**, 2484–2492.
26 R. C. Jeske, J. M. Rowley and G. W. Coates, *Angew. Chem., Int. Ed.*, 2008, **47**, 6041–6044.
27 A. J. Plajer and C. K. Williams, *Angew. Chem., Int. Ed.*, 2021, **60**, 13372–13379.
28 S. Huijser, E. HosseiniNejad, R. Sablong, C. de Jong, C. E. Koning and R. Duchateau, *Macromolecules*, 2011, **44**, 1132–1139.
29 Y. Liu, J.-Z. Guo, H.-W. Lu, H.-B. Wang and X.-B. Lu, *Macromolecules*, 2018, **51**, 771–778.
30 Z. Yang, C. Hu, F. Cui, X. Pang, Y. Huang, Y. Zhou and X. Chen, *Angew. Chem., Int. Ed.*, 2022, **61**, e202117533.
31 J. Xu, X. Wang and N. Hadjichristidis, *Nat. Commun.*, 2021, **12**, 7124.
32 G. Rosetto, A. C. Deacy and C. K. Williams, *Chem. Sci.*, 2021, **12**, 12315–12325.
33 J. Tang, M. Li, X. Wang and Y. Tao, *Angew. Chem., Int. Ed.*, 2022, e202115465.
34 X. Wang and R. Tong, *J. Am. Chem. Soc.*, 2022, **144**, 20687–20698.
35 C. Romain, Y. Zhu, P. Dingwall, S. Paul, H. S. Rzepa, A. Buchard and C. K. Williams, *J. Am. Chem. Soc.*, 2016, **138**, 4120–4131.
36 F. N. Singer, A. C. Deacy, T. M. McGuire, C. K. Williams and A. Buchard, *Angew. Chem., Int. Ed.*, 2022, e202201785.
37 Y. Liu, H. Zhou, J.-Z. Guo, W.-M. Ren and X.-B. Lu, *Angew. Chem., Int. Ed.*, 2017, **56**, 4862–4866.
38 J.-L. Yang, H.-L. Wu, Y. Li, X.-H. Zhang and D. J. Darensbourg, *Angew. Chem., Int. Ed.*, 2017, **56**, 5774–5779.
39 T.-J. Yue, M.-C. Zhang, G.-G. Gu, L.-Y. Wang, W.-M. Ren and X.-B. Lu, *Angew. Chem.*, 2019, **131**, 628–633.
40 W.-M. Ren, J.-Y. Chao, T.-J. Yue, B.-H. Ren, G.-G. Gu and X.-B. Lu, *Angew. Chem., Int. Ed.*, 2022, **61**, e2021159.
41 L.-Y. Wang, G.-G. Gu, B.-H. Ren, T.-J. Yue, X.-B. Lu and W.-M. Ren, *ACS Catal.*, 2020, **10**, 6635–6644.
42 Y. Wang, Y. Zhu, W. Lv, X. Wang and Y. Tao, *J. Am. Chem. Soc.*, 2023, **145**(3), 1877–1885.
43 T.-J. Yue, G. A. Bhat, W.-J. Zhang, W.-M. Ren, X.-B. Lu and D. J. Darensbourg, *Angew. Chem., Int. Ed.*, 2020, **59**, 13633–13637.
44 T.-J. Yue, M.-C. Zhang, G.-G. Gu, L.-Y. Wang, W.-M. Ren and X.-B. Lu, *Angew. Chem., Int. Ed.*, 2019, **58**, 618–623.
45 X.-F. Zhu, G.-W. Yang, R. Xie and G.-P. Wu, *Angew. Chem., Int. Ed.*, 2022, e202115189.
46 J. Diebler, H. Komber, L. Häußler, A. Lederer and T. Werner, *Macromolecules*, 2016, **49**, 4723–4731.
47 L.-Y. Wang, G.-G. Gu, T.-J. Yue, W.-M. Ren and X.-B. Lu, *Macromolecules*, 2019, **52**, 2439–2445.
48 X.-L. Chen, B. Wang, D.-P. Song, L. Pan and Y.-S. Li, *Macromolecules*, 2022, **55**, 1153–1164.
49 S. Rupf, P. Pröhm and A. J. Plajer, *Chem. Sci.*, 2022, **13**, 6355–6365.
50 D. Silbernagl, H. Sturm and A. J. Plajer, *Polym. Chem.*, 2022, **13**, 3981–3985.
51 A. J. Plajer, *ChemCatChem*, 2022, **14**, e2022008.
52 F. Furche, R. Ahlrichs, C. Hättig, W. Klopper, M. Sierka and F. Weigend, *WIREs Comput. Mol. Sci.*, 2014, **4**, 91.
53 J. Tao, J. Perdew, V. Staroverov and G. Scuseria, *Phys. Rev. Lett.*, 2003, **91**, 146401.
54 V. Staroverov, G. Scuseria, J. Tao and J. Perdew, *J. Chem. Phys.*, 2003, **119**, 12129.
55 A. Schäfer, C. Huber and R. Ahlrichs, *J. Chem. Phys.*, 1994, **100**, 5829.
56 A. Klamt and G. Schüürmann, *J. Chem. Soc., Perkin Trans. 2*, 1993, 799.
57 Y. Zhao and D. G. Truhlar, *Theor. Chem. Acc.*, 2008, **120**, 215.
58 F. Weigend and R. Ahlrichs, *Phys. Chem. Chem. Phys.*, 2005, **7**, 3297.
59 F. Eckert and A. Klamt, *AIChE J.*, 2002, **48**, 369.